ISSN: 0975-833X

Available online at http://www.journalcra.com

International Journal of Current Research
Vol. 14, Issue, 08, pp.22053-22058, August, 2022
DOI: https://doi.org/10.24941/ijcr.43876.08.2022

INTERNATIONAL JOURNAL OF CURRENT RESEARCH

RESEARCH ARTICLE

CHARACTERISTICS OF MAGNETIC FIELD SIGNAL DISTRIBUTION OF DOUBLE-ASSOCIATED DEFECTS BASED ON METAL MAGNETIC MEMORY

***Daluan Wang and Shangkun Ren**

Key Laboratory of Non-destructive Testing Technology of Ministry of Education, School of Testing and Optoelectronic Engineering, Nanchang Hangkong University, Nanchang 330063, Jiangxi, China

ARTICLE INFO

Article History:
Received 09th May, 2022
Received in revised form
15th June, 2022
Accepted 14th July, 2022
Published online 23rd August, 2022

Key words:

Metal Magnetic Memory Detection; double-association defect; magnetic dipole; Magnetic memory signal.

**Corresponding Author:*
Daluan Wang

ABSTRACT

In order to study the magnetic field distribution characteristics of double-correlated defects, the ferromagnetic specimen is simulated and analyzed by MATLAB based on the principle of magnetic dipole, and the analytical expression of the leakage magnetic field strength at any point in the air of the specimen with double-defects is obtained. Through numerical calculation with MATLAB, the influence rule of defect width, defect depth and double-correlated defect spacing on magnetic memory signal is obtained. At the same time, the first-order differential curve of magnetic memory signal and Lissajous figure are introduced to further verify the correctness of the conclusion, which is suitable for practical engineering applications. Provide reference for defect detection of medium ferromagnetic materials.

Citation: ***Daluan Wang andShangkun Ren.*** **2022**. "Characteristics of Magnetic Field Signal Distribution of Double-Associated Defects Based on Metal Magnetic Memory*". International Journal of Current Research*, 14, (08), 22053-22058.

INTRODUCTION

Ferromagnetic materials have good mechanical properties such as brittleness, toughness, and strength (Li yafeng, 2018), and are widely used in all walks of life. The failure or even fracture of ferromagnetic materials (Zhao shuaijie, 2022; Zhang bo, 2020; Bao sheng, 2021), serious or even catastrophic accidents, seriously threaten the safety of people's property and life, and cause huge losses to the national economy. If the hidden damage of ferromagnetic specimens in engineering can be discovered in time, and repaired and prevented to avoid accidents, it is of great significance to people's happy life, social harmony and stability, and the rapid development of the country. Metal magnetic memory detection technology was developed at the end of the 20th century. Compared with other detection technologies, it has the advantages of no excitation source and no surface treatment (Ren jilin, 2016).

The metal magnetic memory detection technology is based on the force-magnetic coupling effect. Under the combined action of the geomagnetic field and stress load, it can realize the early diagnosis of the stress concentration and damage degree of the ferromagnetic specimen, which can effectively prevent the occurrence of disasters (Liu bin, 2014; Zhang peng, 2013). At present, the research on metal magnetic memory detection mainly focuses on three aspects: exploratory experiment, establishment of theoretical model and development of instruments and equipment. For example, Jiles (2004) studied the magnetostrictive effect, proposed the famous J-A model, and defined The magneto-mechanical effect was studied; Ren Shangkun *et al*. (2022) studied the force-magnetic coupling effect of different types of notches, and used the changes of the magnetic memory signal in the elastic and plastic stages to identify the defect damage of the engineering specimen early; Ren Jilin *et al*. (2010) A new type of magnetoresistive sensor HMC1002 is designed by the method of combined normal and tangential detection, which has good application value in the quantitative analysis of magnetic memory detection; Minhhuy Le *et al*. (2013). The dipole model method estimates the shape and volume of the crack, which is consistent with the experimental results. In this paper, the magnetic dipole principle is used to obtain the leakage magnetic field strength at any point in the space of a ferromagnetic specimen with double-correlated defects, and MATLAB is used to simulate and analyze the spatial leakage magnetic field of the specimen, and the defect depth and defect width are discussed in detail. The influence of the distance between the two defects on the spatial leakage magnetic field signal provides a theoretical basis for the quantitative detection of defects.

Double-correlated defect magnetic dipole model: The schematic diagram of double-related defects is shown in Fig.1. The two defects are located on both sides of the Y-axis, the distance between the rectangular defect and the V-shaped defect is 2m, the depth of the two defects is h, and the length is 2b,the thickness is H.

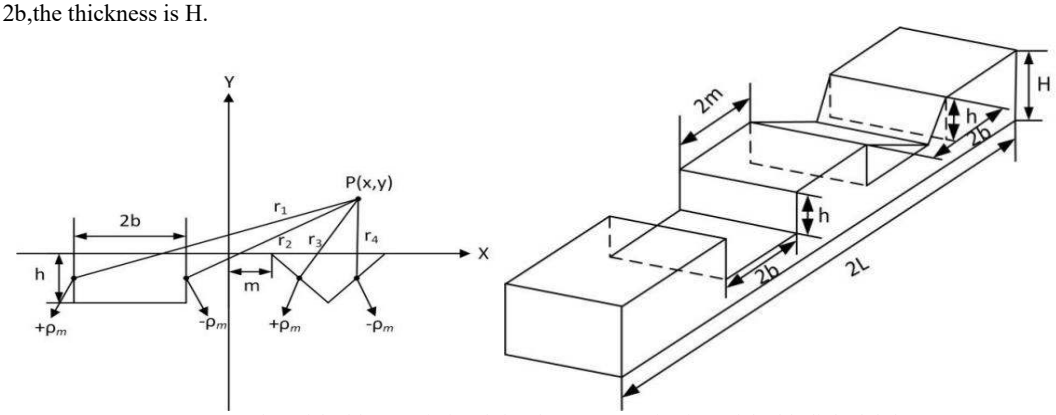

(a) Plan of double-associative defect(b) Stereoscopic view of double-linked defect

Fig. 1. Schematic diagram of double-associative defect

Under the action of tensile stress and geomagnetic field, the specimen is approximately magnetized into a magnet. Assuming that the left end of the rectangular defect has a positive magnetic charge, the right end of the V-shaped defect has an equal amount of negative magnetic charge, and the two magnetic charges are in their respective grooves. A new equal amount of heterogeneous magnetic charge is induced in the groove, and the magnetic charge is uniformly distributed in the groove. Under the action of tensile stress, stress concentration occurs in the defective part of the ferromagnetic specimen, and a leakage magnetic field is generated in the air that is different from the defect-free one. The defect location can be realized by extracting the variation characteristics of the leakage magnetic field. The leakage magnetic field strength of any point P in space can be expressed as:

$$H_x = H_{x0} - \frac{\rho_m}{2\pi\mu_0}\left(\int_{-h}^{0}\frac{x+m+2b}{(x+m+2b)^2+(y-a)^2}da + \int_{-h}^{0}\frac{m+\frac{ab}{h}-x}{\left(m+\frac{ab}{h}-x\right)^2+(y-a)^2}da - \int_{-h}^{0}\frac{x+m}{(x+m)^2+(y-a)^2}da - \int_{-h}^{0}\frac{m+2b-\frac{ab}{h}-x}{\left(m+2b-\frac{ab}{h}-x\right)^2+(y-a)^2}da\right) \tag{1}$$

$$= H_{x0} - \frac{\rho_m}{2\pi\mu_0}\left(\begin{array}{l}\arctan\frac{h+y}{2b+m+x} - \arctan\frac{y}{2b+m+x} - \arctan\frac{h+y}{m+x} + \arctan\frac{y}{m+x} - \frac{h^2\arctan\frac{bm-bx+hy+3b^2+h^2}{2bh+hm-by-hx} - h^2\arctan\frac{bx-bm+hy+b^2+h^2}{hm+by-hx}}{b^2+h^2} \\ -\frac{h^2\arctan\frac{-bm+bx+hy}{hm+by-hx} - h^2\arctan\frac{-bx+bm+hy+2b^2}{2bh+hm-by-hx}}{b^2+h^2} - \frac{bh\log\left(h^2\left(b^2-2bm+2bx+h^2+2hy+m^2-2mx+x^2+y^2\right)\right)}{2b^2+2h^2} \\ +\frac{bh\log\left(h^2\left(4b^2+4bm-4bx+m^2-2mx+x^2+y^2\right)\right)}{2b^2+2h^2} + \frac{bh\log\left(h^2\left(m^2-2mx+x^2+y^2\right)\right)}{2b^2+2h^2} - \frac{bh\log\left(h^2\left(9b^2+6bm-6bx+h^2+2hy+m^2-2mx+x^2+y^2\right)\right)}{2b^2+2h^2}\end{array}\right) \tag{2}$$

$$H_y = H_{y0} - \frac{\rho_m}{2\pi\mu_0}\left(\int_{-h}^{0}\frac{y-a}{(x+m+2b)^2+(y-a)^2}da + \int_{-h}^{0}\frac{y-a}{\left(m+\frac{ab}{h}-x\right)^2+(y-a)^2}da - \int_{-h}^{0}\frac{y-a}{(x+m)^2+(y-a)^2}da - \int_{-h}^{0}\frac{y-a}{\left(m+2b-x-\frac{ab}{h}\right)^2+(y-a)^2}da\right) \tag{3}$$

$$= H_{y0} - \frac{\rho_m}{2\pi\mu_0}\left(\begin{array}{l}\frac{\log\left(4b^2+4bm+4bx+h^2+2hy+m^2+2mx+x^2+y^2\right)}{2} - \frac{\log\left(4b^2+4bm+4bx+m^2+2mx+x^2+y^2\right)}{2} \\ +\frac{\log\left(m^2+2mx+x^2+y^2\right)}{2} - \frac{\log\left(h^2+2hy+m^2+2mx+x^2+y^2\right)}{2} \\ -\frac{h^2\log\left(h^2\left(m^2-2mx+x^2+y^2\right)\right)}{2b^2+2h^2} + \frac{h^2\log\left(h^2\left(b^2-2bm+2bx+h^2+2hy+m^2-2mx+x^2+y^2\right)\right)}{2b^2+2h^2} \\ +\frac{h^2\log\left(h^2\left(4b^2+4bm-4bx+m^2-2mx+x^2+y^2\right)\right)}{2b^2+2h^2} \\ -\frac{h^2\log\left(h^2\left(9b^2+6bm-6bx+h^2+2hy+m^2-2mx+x^2+y^2\right)\right)}{2b^2+2h^2} \\ -\frac{bh\arctan\frac{bx-bm+hy}{hm+by-hx} + bh\arctan\frac{bm-bx+hy+2b^2}{2bh+hm-by-hx}}{b^2+h^2} \\ +\frac{bh\arctan\frac{-bx+bm+hy+3b^2+h^2}{hm-by-hx+2bh} + bh\arctan\frac{-bm+bx+hy+b^2+h^2}{hm+by-hx}}{b^2+h^2}\end{array}\right) \tag{4}$$

Analysis and discussion of the influence of defect characteristic parameters on the leakage magnetic field signal: The model parameters of the magnetic dipole are set as shown in Table 1. The selected model parameters are the results after many tests. When the defect parameters change, the forward model can well reflect the change of the defect. Table 1 shows the default values of model parameters, that is, when one parameter value is changed, other parameters are default values.

Table 1. Parameter table of magnetic dipole model

Magnetic Dipole Model Parameters	Numerical value	Magnetic Dipole Model Parameters	Numerical value
Vacuum permeability$\boldsymbol{\mu_0}$	$4\pi \times 10^{-7}\mathrm{N/A^2}$	Defect depth$h$	1mm
Magnetization$M$	$5.4 \times 10^{3}\mathrm{A/m}$	Specimen half length$L$	200mm
lift off height$y$	1mm	Specimen thickness$H$	3mm
Defect half width$b$	0.3mm	Double defect spacing$2m$	6mm

Influence of defect width on leakage magnetic field: Fig.2 shows the effect of defect width on the magnetic memory signal. The tangential and normal components of the magnetic memory signal show a nonlinear change with the change of displacement, which increases first, then decreases and then increases; when the defect width increases, The peak points of the tangential and normal components of the magnetic memory signal move up, indicating that the stress concentration at the defect is more obvious, and the tangential component of the magnetic memory signal has a maximum value. The basic detection characteristics of the technology.

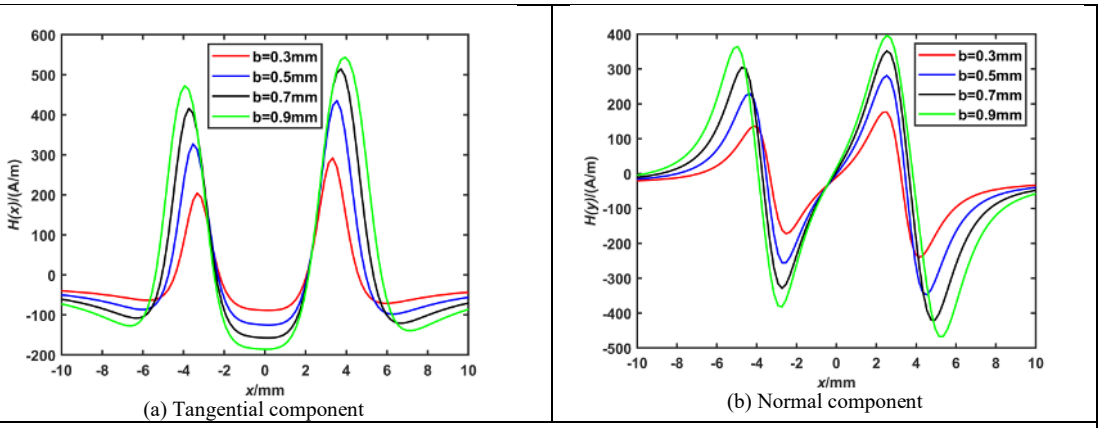

(a) Tangential component (b) Normal component

Fig.2. Distribution curve of leakage magnetic field intensity with defect width

Fig.3 shows the influence of the defect width on the first differential value of the magnetic memory signal. Since the metal magnetic memory detection is a weak magnetic detection, it is easy to receive interference from external factors. If only the tangential and normal components of the magnetic memory signal are used to judge the curve The position is prone to misjudgment and missed detection, so the first-order differential curve is introduced as the eigenvalue to determine the stress concentration. It can be seen from Fig.3 that with the increase of the displacement, the first-order differential curve of the tangential component of the magnetic memory signal shows a trend of first increasing, then decreasing, and then increasing at the defect, and at the zero-crossing point; the first-order differential curve of the normal component of the magnetic memory signal The defect shows a trend of first decreasing and then increasing, and there is a maximum value. As the defect width increases, the peak-to-valley value of the first-order differential curve also increases, which is consistent with the defect characteristics described in Fig.2, which further verifies the correctness of the model. Fig.4 is a two-dimensional curve synthesized by the first-order differential curve of the magnetic memory signal changing with the defect width, that is, a Lissajous figure.

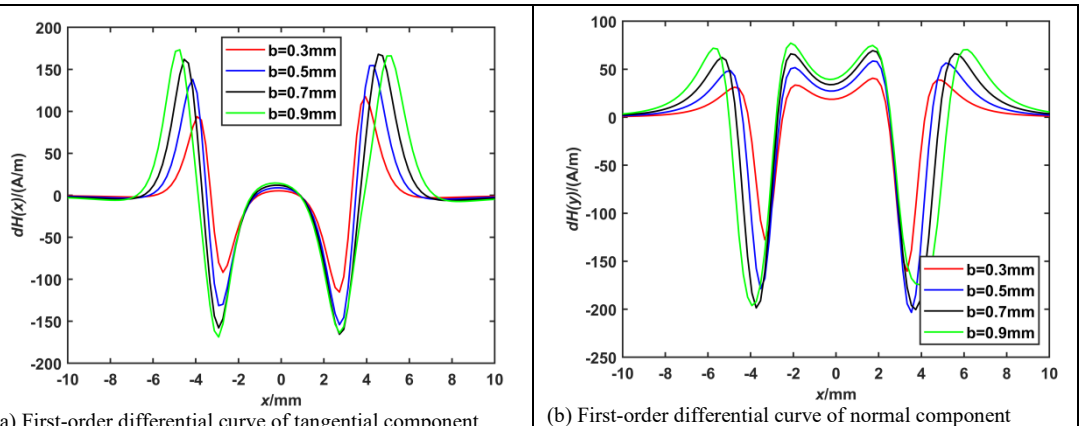

(a) First-order differential curve of tangential component (b) First-order differential curve of normal component

Fig. 3. First-order differential distribution curve of leakage magnetic field intensity as a function of defect width

As the defect width increases, the closed Lissajous area also increases, and as the defect width increases by an equal amount, the change rate of the Lissajous area decreases gradually, which is consistent with Figure 3. When the defect width is the same, the ellipse with a small area is formed by a rectangular defect, and the ellipse with a large area is formed by a V-shaped defect, indicating that the V-shaped defect is easier to detect than the rectangular defect.

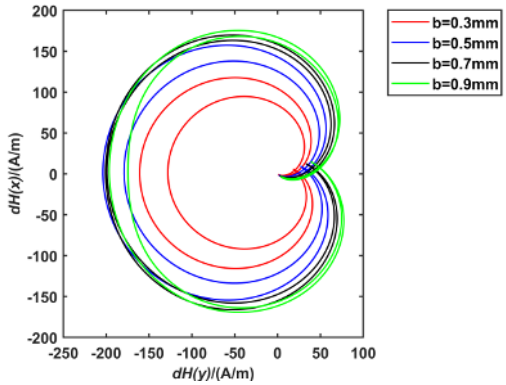

Fig.4. Lissajous figure under different defect widths

Influence of defect depth on leakage magnetic field signal: Fig.5 shows the effect of defect depth on the magnetic memory signal. With the increase of the defect depth, the peaks of the tangential and normal components of the magnetic memory signal gradually increase, that is, the deeper the defect, the easier it is to detect, and the increase of the defect depth only Changing the amplitude of the curve does not change the trend of the curve. The maximum value of the tangential component of the rectangular defect is about 300A/m, the maximum value of the tangential component of the V-shaped defect is about 400A/m, and the extreme points of the rectangular defect and the V-shaped defect appear at -3mm and 3mm, satisfying the two defects. Constraints of 6mm spacing.

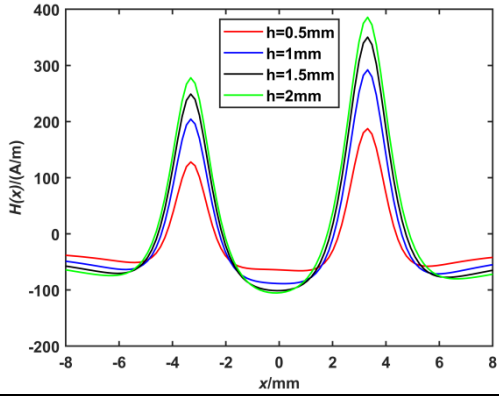

(a) Tangential component

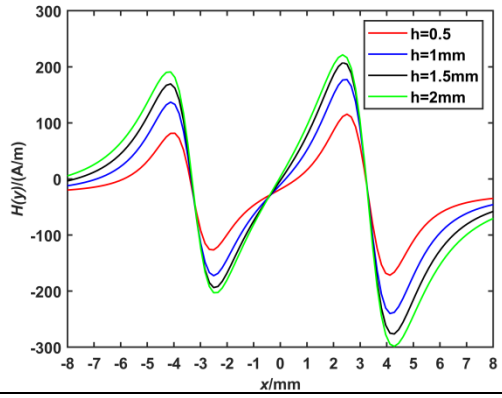

(b) Normal component

Fig.5 Distribution curve of leakage magnetic field intensity as a function of defect width

Fig.6 shows the influence of the defect depth on the first differential value of the magnetic memory signal. The first differential curve of the tangential component of the magnetic memory signal crosses the zero point, and the first differential curve of the normal component has a maximum value, which can well reflect the location of the defect. With the increase of the displacement, the peak and valley values of the two components both increase, and the first-order differential curve of the normal component at the V-shaped defect diverges in a butterfly shape, which is consistent with the stress concentration cloud diagram of the V-shaped defect, indicating that the leakage magnetic field appears. The essence is that the ferromagnetic specimen has stress concentration phenomenon.

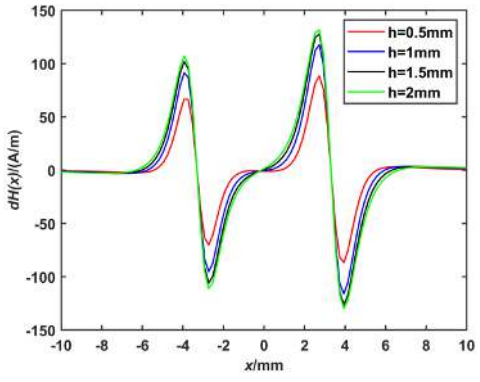

(a) First-order differential curve of tangential component

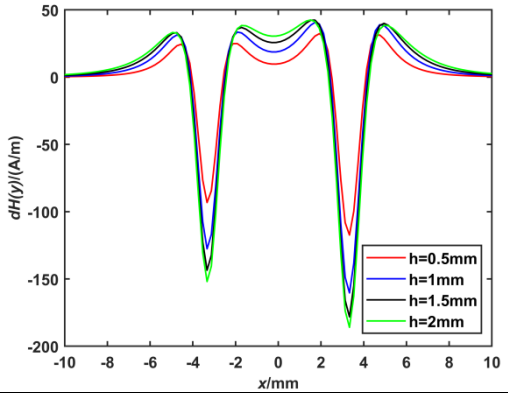

(b) First-order differential curve of normal component

Fig.6. First-order differential distribution curve of leakage magnetic field intensity as a function of defect depth

Fig.7 is a two-dimensional curve synthesized by the first-order differential curve of the magnetic memory signal changing with the depth of the defect. As the depth of the defect increases, the increase rate of the Lissajous area gradually decreases, and the smaller ellipse is generated by the rectangular defect. Larger ellipses are produced by V-shaped defects. The size of the closed area of the Lissajous figure can be used to judge the

difficulty of stress concentration at the buried defect of the test piece. The introduction of the Lissajous figure combines the primary differential component of the magnetic memory signal to avoid misjudgment and missed detection due to a single component.

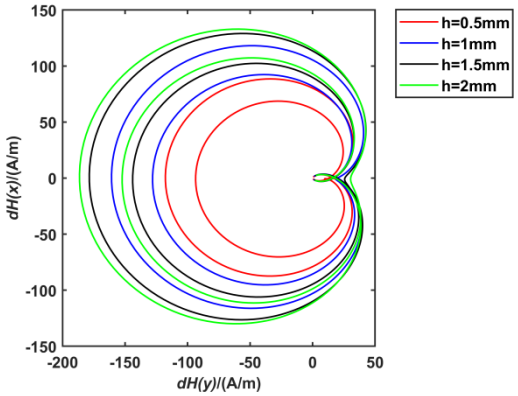

Fig.7. Lissajous figure at different defect depths

Influence of double defect spacing on leakage magnetic field signal: Fig.8 shows the effect of the double-defect spacing on the magnetic memory signal. When the double-related defect spacing increases, the peak value of the magnetic memory signal gradually increases. Therefore, the larger the distance between the two defects, the easier the defect is to be detected. This is because the stress concentration of the double-correlated specimen is less than that of a single notch due to the superposition of multiple magnetic and magnetic effects at the notch. In the process of gradually increasing the m value, this magnetic and magnetic effect gradually weakens. As a result, the larger the m value, the larger the peak value of the magnetic memory signal. The extreme point of the tangential component and the peak point of the normal component of the magnetic memory signal continuously move to both sides with the increase of the distance between the two defects, which can well reflect the position of the defect.

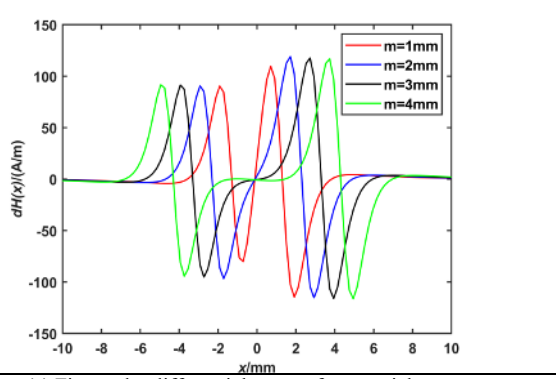

(a) First-order differential curve of tangential component

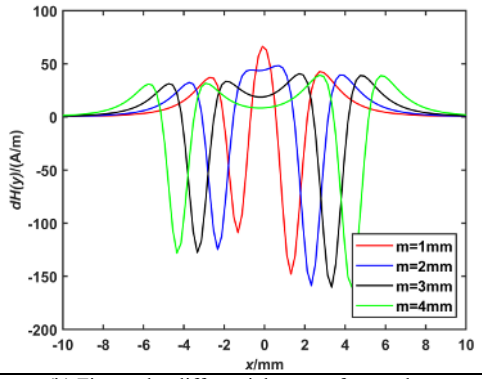

(b) First-order differential curve of normal component

Fig.9 The first-order differential distribution curve of the leakage magnetic field intensity as a function of the double-defect spacing

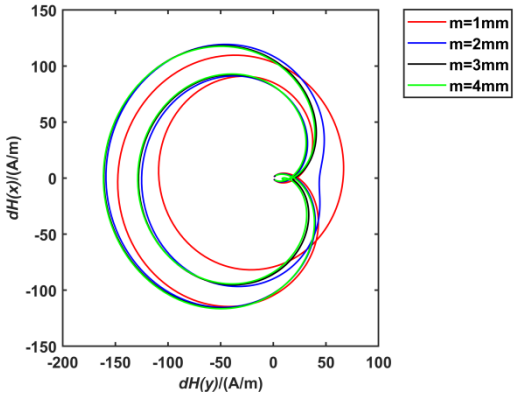

Fig. 10. Lissajous figure under the variation of double defect spacing

Fig.9 shows the influence of the double defect spacing on the first-order differential value of the magnetic memory signal. The variation trend of the first-order differential curve of the leakage magnetic field strength is opposite to the leakage magnetic field strength, that is, both H(x) and dH(y) have extreme points, and H(y) Both dH(x) and dH(x) cross the zero point and show a center-symmetrical trend, so this feature can be used to locate defects. When the double-related defect spacing increases, the change trend of the first-order differential curve remains unchanged, and the size changes. Therefore, the change of the double-related defect spacing only affects the value and does not affect the change trend. When the

double-related defect spacing is greater than 2mm, the first-order differential of the magnetic signal The curve values are hardly affected by the spacing and tend to be stable. Fig.10 is the two-dimensional curve synthesized by the first-order differential curve of the magnetic memory signal with the double-defect spacing. When the double-defect spacing increases, the area of the closed area of the Lissajous figure increases, that is, the possibility of stress concentration increases. Therefore, the introduction of Lissajous figures provides a basis for judging the fracture position of ferromagnetic specimens under stress conditions. When the distance between the double-related defects is greater than 2mm, the area of the Lissajous figure hardly increases with the increase of the distance. Therefore, in practical engineering, for two defects with a width of 0.6mm and a depth of 1mm, when the distance is greater than 2mm, the fractured The most dangerous.

CONCLUSION

In this paper, the magnetic dipole principle is used to obtain the leakage magnetic field strength at any point in the space of the ferromagnetic specimen with double-correlated defects, and the spatial leakage magnetic field of the specimen is simulated and analyzed by MATLAB, and the defect width, defect depth and double leakage magnetic field are obtained. The influence law of the associated defect spacing on the magnetic memory signal, the first derivative of the magnetic memory signal and the Lissajous figure. The results show that the defect width, defect depth and double associated spacing only affect the value of the magnetic memory signal, but do not affect its variation law. And the larger the defect width and the deeper the depth, the more obvious the stress concentration of the ferromagnetic specimen is under the action of the tensile stress and the geomagnetic field, and the larger the peak value of the magnetic memory signal. The distance increases with the increase of the distance. When the distance between the double-associated defects is greater than 2 mm, the peak value of the magnetic memory signal gradually tends to be stable with the increase of the distance. At the same time, the introduction of the first-order differential curve avoids the possibility of misjudgment and missed detection due to a single criterion. The larger the area of the Lissajous figure, the easier it is for the ferromagnetic specimen to generate stress concentration there.

REFERENCES

Bao Sheng, Zhao Zhengye, Luo Qiang. 2021. Influence of stress loading history on the evolution of piezomagnetic field of ferromagnetic materials(J).Engineering Mechanics, 38(S1):259-263.

Jiles D C. LI L. 2004. A new approach to modeling the magneto-mechanical effect(J).Journal of Applied Physics.95(11):7085-7060

Li Yafeng. 2018. Analysis of the current situation and development prospects of the magnetic material industry(J)Advanced Materials Industry. (07):51-54.

Liu Bin, Zhang Wei, Yang Minghan, *et al*. 2014. Study on the Force-Magnetic Coupling Model Based on First-Principle(J)Instrument Technique and Sensor. (03):76-78.

Minhhuy Le, Jinyi Lee, Jongwoo Jun, *et al*. 2013. Hall sensor array based validation of estimation of crack size in metals using magnetic dipole models(J). NDT & E International, (53):18-25.

Ren Jilin, Liu Haichao, Song Kai. 2016. The Rise and Development of Metal Magnetic Memory Testing Technology(J).nondestructive testing, ,38(11):7-15.

Ren jilin, Wang jin,Fan zhenzhong, *et al*. 2010. New method for metal magnetic memory quantitative analysis(J).Chinese Journal of Scientific Instrument,31(02):431-436

Wang daluan, Ren shangkun, Deng keyu, *et al*. 2022. Study on the influence of notch type of ferromagnetic specimen on magnetic memory signal(J/OL).CHINA MEASUREMENT & TEST:1-7.

Zhang Bo, Huo tianlong. 2020. Research on surface inspection of ferromagnetic material welds(J).Journal of Guilin University of Aerospace Technology, 25 (04) :449-452.

Zhang Peng, Liu lin, Chen Weimin. 2013. Analysis of characteristics and key influencing factors in magnetomechanical behavior for cable stress monitoring(J).Acta Physica Sinica,62(17):454-462.

Zhao shuaijie, Zhang jitang, Zhou junfeng, *et al*. 2022. Research on the change law of sound velocity based on high temperature EMAT ferromagnetic material(J/OL).CHINA MEASUREMENT & TEST:1-8.

****